Bulletin of the Seismological Society of America. Vol. 60, No. 1, pp. 137–160. February, 1970

COMPLEXITY OF ENERGY RELEASE DURING THE IMPERIAL VALLEY, CALIFORNIA, EARTHQUAKE OF 1940

By Mihailo D. Trifunac and James N. Brune

ABSTRACT

The pattern of energy release during the Imperial Valley, California, earthquake of 1940 is studied by analyzing the El Centro strong motion seismograph record and records from the Tinemaha seismograph station, 546 km from the epicenter. The earthquake was a multiple event sequence with at least 4 events recorded at El Centro in the first 25 seconds, followed by 9 events recorded in the next 5 minutes. Clear *P*, *S*, and surface waves were observed on the strong motion record. Although the main part of the earthquake energy was released during the first 15 seconds, some of the later events were as large as $M = 5.8$ and thus are important for earthquake engineering studies. The moment calculated using Fourier analysis of surface waves agrees with the moment estimated from field measurements of fault offset after the earthquake. The earthquake engineering significance of the complex pattern of energy release is discussed. It is concluded that a cumulative increase in amplitudes of building vibration resulting from the present sequence of shocks would be significant only for structures with relatively long natural period of vibration. However, progressive weakening effects may also lead to greater damage for multiple event earthquakes.

Nomenclature

A	Area of the fault plane over which slip occurs
$A(t)$	Envelope of the vibration amplitude
$a(t)$	Window amplitude
A_L	Love wave amplitude factor
b	Fault length
C	Phase velocity
$F(\omega, t^*, \Delta t)$	Moving window Fourier spectrum
f	Frequency
$f(t), f^*_{\Delta t}(t)$	Instrument record trace
M_0	Seismic moment associated with a double couple source
$M^i_{0\text{-SEISM}}$, $M^{\text{TOT}}_{0\text{-SEISM}}$, $M_{0\text{-FIELD}}$	Seismic moment of a single event, seismic moment of all events and the total field moment, respectively
$M_L^{\text{S.M.}}$	Local magnitude estimated using the strong motion instrument
p	Circular frequency of vibration of a one degree of freedom system
Q	Attenuation constant
T	Period $(=2\pi/\omega)$
T_0	Period at which moment is evaluated
t	Time coordinate
t^*	Center time of moving Fourier window
$t_{1/20}$	Time at which the vibration amplitude has decreased to 1/20 of the initial value

U	Group velocity
u_θ^{dc}	Component of the displacement field in θ direction due to a double couple source
u	Spectral density determined from the record
$\bar{u}$	Weighted average of the fault slip
v	Velocity of source propagation
$W_{\Delta t}(t^*)$	Window amplitude
x	Characteristic coordinate describing the vibration of a one degree of freedom system
α	Compressional wave velocity
β	Shear wave velocity
δ	Angle between u_θ^{dc} and EW component
θ	Strike direction
Δ	Source distance
Δt	Window width
ζ	Fraction of the critical damping
μ	Rigidity
ρ	Density
ω	Circular frequency $(=2\pi f)$

Other symbols not defined here are given in the text with an appropriate explanation.

Introduction

In this study we analyze records of the Imperial Valley, California earthquake of 1940 to obtain information about the complexity of the source function in time and space. The results of the study indicate that the Imperial Valley earthquake was characterized by multiple events that occurred in the first 15 seconds and several later events (in the next 5 minutes) which could be called aftershocks, but which, in some cases, were comparable in magnitude to the events in the main sequence. Thus this earthquake, which has often been described in earthquake engineering studies as a typical moderate-sized destructive earthquake, had a complicated pattern of energy release. Numerous examples of a complex pattern of energy release for larger earthquakes may be found in the literature (Florensov and Solonenko, 1963; Wyss and Brune, 1967; among others).

It may be noted here that the meaning of an "event" as it will be used throughout this paper will be associated with any occurrence of energy release which generates seismic phases that can be resolved and identified. This of course depends much on the frequency resolution of the recording instrument and its distance from the source of the energy release. We will call a sequence of P, S, and surface waves an "event" if the P and S waves each represent a single resolvable burst of incoming energy which might be associated with a relatively discrete single dislocation. Thus erratic propagation of a dislocation along a single fault plane may generate a series of "events."

The Imperial Valley earthquake was centered along a well defined fault, and after the earthquake the fault offset was documented in detail (Buwalda, unpublished field notes; Richter, 1958). This allows estimation of the moment from field evidence, and thus gives an independent check on the results obtained from the instrumental records. The El Centro strong motion accelerogram used in this study, has a special significance for earthquake engineering, since, considering both duration and amplitude, it is the strongest earthquake ground motion yet recorded.

Documentation of the pattern of energy release is important for engineering appli-

cations, first, because the duration and the character of shaking are important factors controlling damage in structures. Secondly, the distance between the source of major energy release and a given structure is clearly closely related to damage.

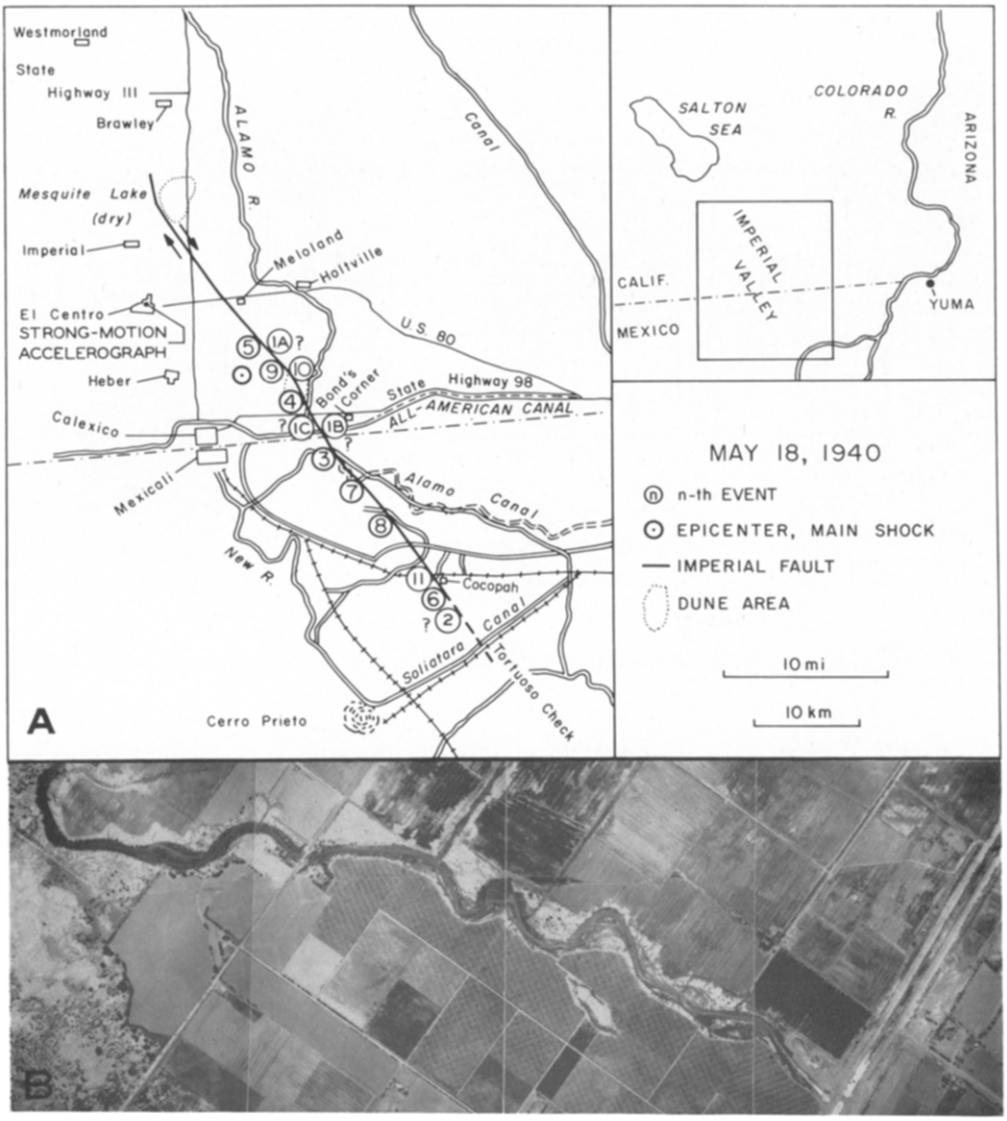

FIG. 1a. Map (after Richter, 1958) indicating the location of the Imperial fault and the epicenter of the main shock. Locations of individual events studied here have been added.
FIG. 1b. Aerial photo of the Imperial fault taken shortly after the 1940 earthquake. The orange grove in this photograph lies south of Cole Road near the point on the fault nearest to Bond's Corner.

DESCRIPTION OF THE IMPERIAL FAULT

The Imperial fault is a northwest trending fault of the San Andreas fault system in southern California. It was discovered as a result of the earthquake of 1940 (Buwalda and Richter, 1941). However, existence of a major structural break along this line is

also indicated by geophysical evidence (Biehler, 1964) as well as by the existence of a pronounced scarp at the northwestern end.

The recent motion along the fault has been almost pure right lateral strike-slip. The fault trace is nearly straight (Figure 1a) except close to the northern end where

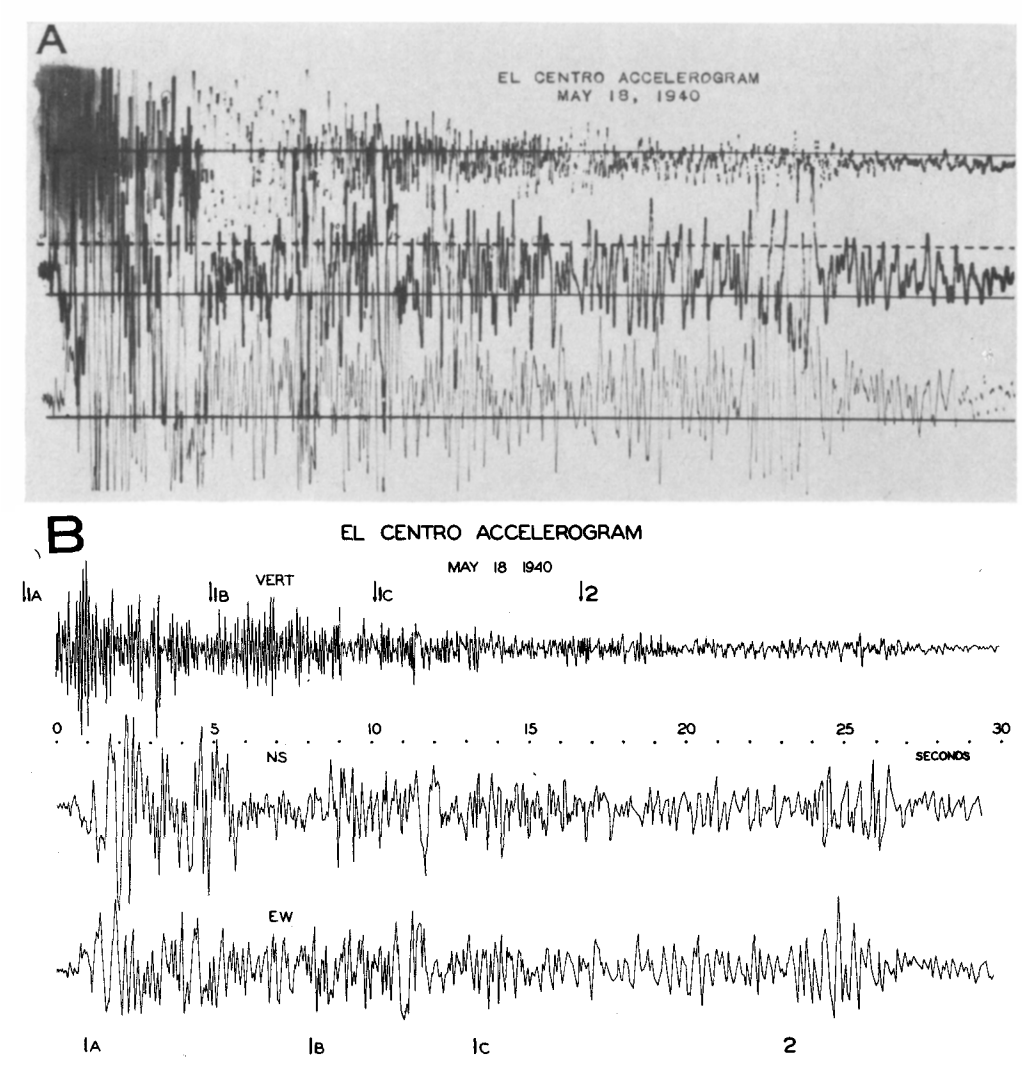

FIG. 2a. El Centro strong motion accelerograph record for events 1A, 1B, 1C and 2. The time is given in seconds.

FIG. 2b. Replotted El Centro strong motion accelerograph record for events 1A, 1B, 1C, and 2. For better readability of the record the gain is reduced by the factor of 2.10.

the fault curves and branches and has a small amount of dip slip. The amount of right lateral motion for the Imperial Valley earthquake has been recorded in detail at various points along the fault (Figure 9; Buwalda, unpublished field notes; Richter, 1958). A map and aerial photo of the fault trace are given in Figures 1a and 1b. The map is modified after Richter (1958). The aerial photo was taken shortly after the 1940 earthquake.

Epicenter of the Main Shock and Aftershocks

Because all close stations were on one side of the epicenter of the main shock, the epicenter could not be determined very accurately. The epicenter given in Richter (1958) is indicated in Figure 1a. Concerning the epicenter of the aftershocks, we quote Richter (1958): "The epicenter of the aftershock at 9:53 p.m. on May 18 cannot be

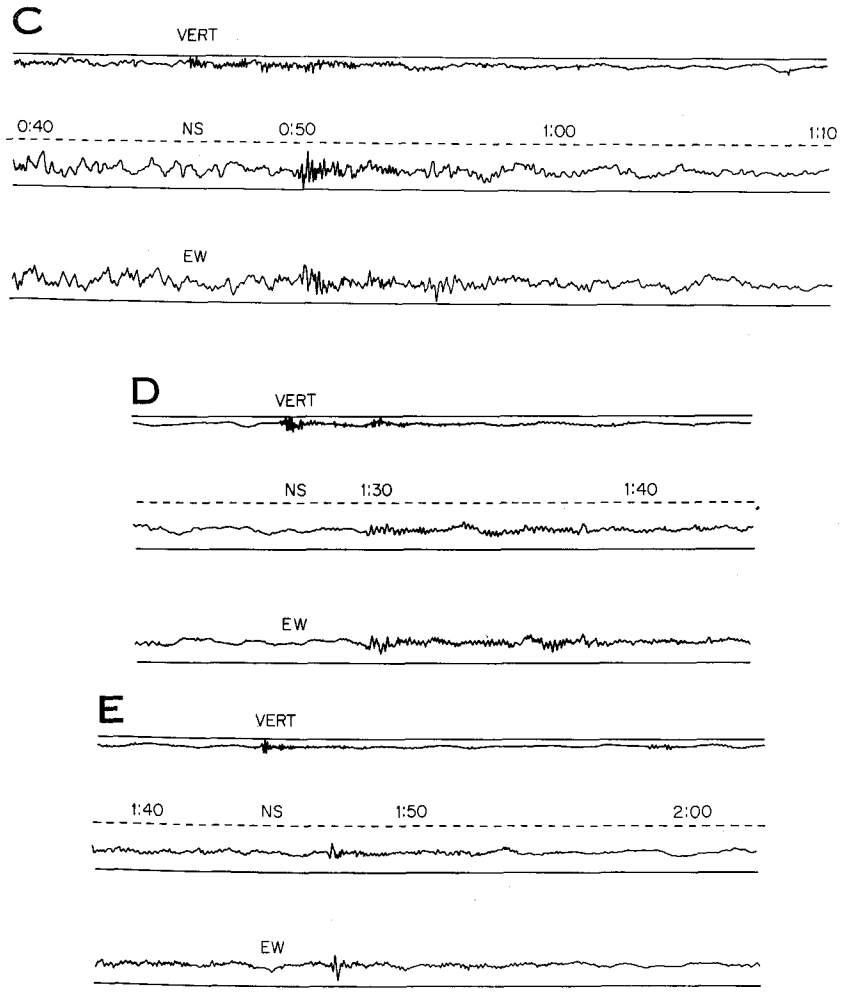

Fig. 2c. El Centro strong motion accelerograph record for event 3.
Fig. 2d. El Centro strong motion accelerograph record for event 4.
Fig. 2e. El Centro strong motion accelerograph record for event 5.

located instrumentally with the desirable precision, nor can any of the immediate aftershocks. Nearly all the large aftershocks were later members of bursts of successive earthquakes, of which the first were too small to be clearly recorded while the later ones were large enough to confuse the recording of the following largest shocks in each group." The Quarterly Bulletin of Local Shocks of the Seismological Laboratory of the California Institute of Technology lists 48 aftershocks in the period 19 May 1940, 4:36 (GCT) to the end of 1940. The first 29 of these recorded aftershocks, with magnitude ranging from 2.0 to 5.5, occurred during the 4 days immediately after the main

shock. In this study we are primarily concerned with the sequence of large events occurring in the first 6 minutes after the origin time of the main event.

Interpretation of the El Centro Strong Motion Record

In order to investigate the nature of energy release in this earthquake, we studied the El Centro strong motion records for the first 6 minutes after the instrument was

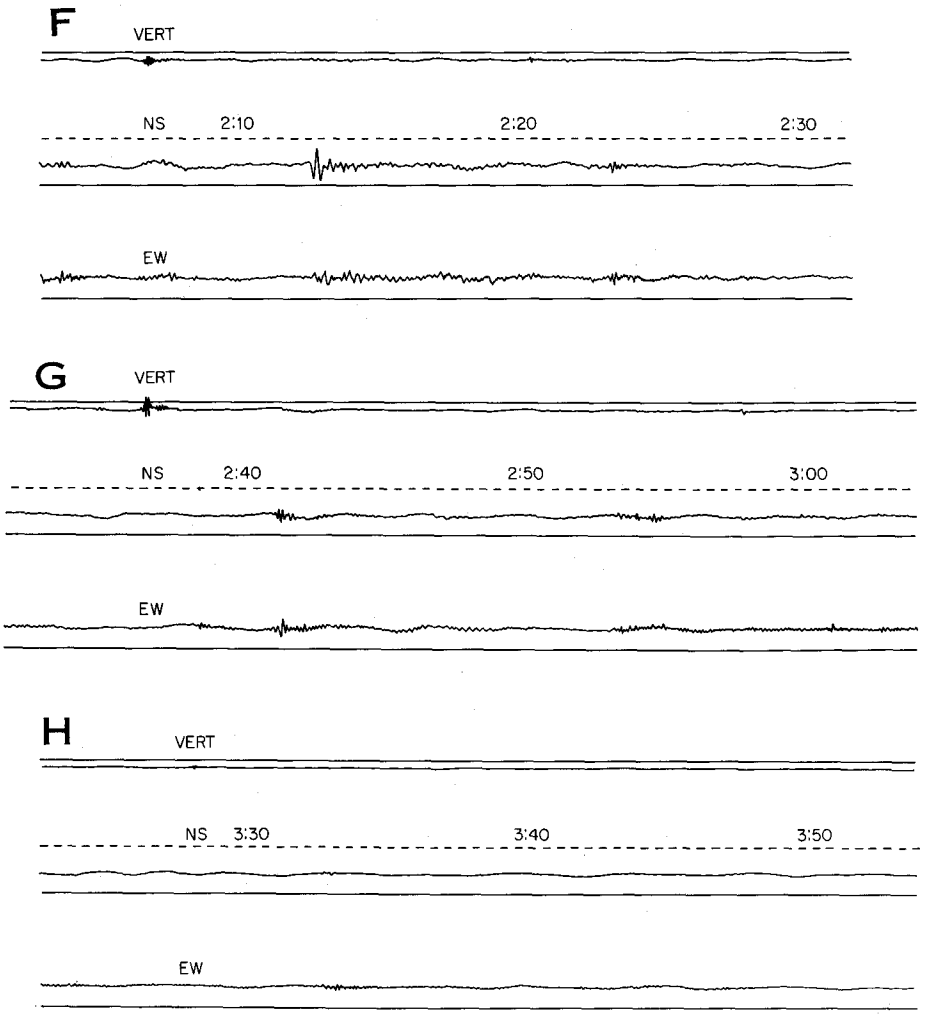

Fig. 2f. El Centro strong motion accelerograph record for event 6.
Fig. 2g. El Centro strong motion accelerograph record for event 7.
Fig. 2h. El Centro strong motion accelerograph record for event 8.

triggered. It is of interest to note that the usually reproduced "standard" accelerogram used for many engineering investigations (Figure 2a) consists only of the first 30 seconds, indicating the first four shocks, and omitting later, also significant, events. The resolution of individual events in a complicated pattern of the energy release is of great importance for this work. Clearly recorded P and S waves, and in most cases, surface waves, were observed for several events. These events are shown in Figures 2a through 2k. The P wave arrived with large amplitudes on the vertical component and

is followed a few seconds later by the S wave which arrived with strong amplitudes on the NS and EW components. Several seconds after the S wave, a longer period (~2 cps) surface wave can clearly be seen for most events. The S-wave amplitudes for events after the first 25 seconds are smaller than those for the earlier events, but when

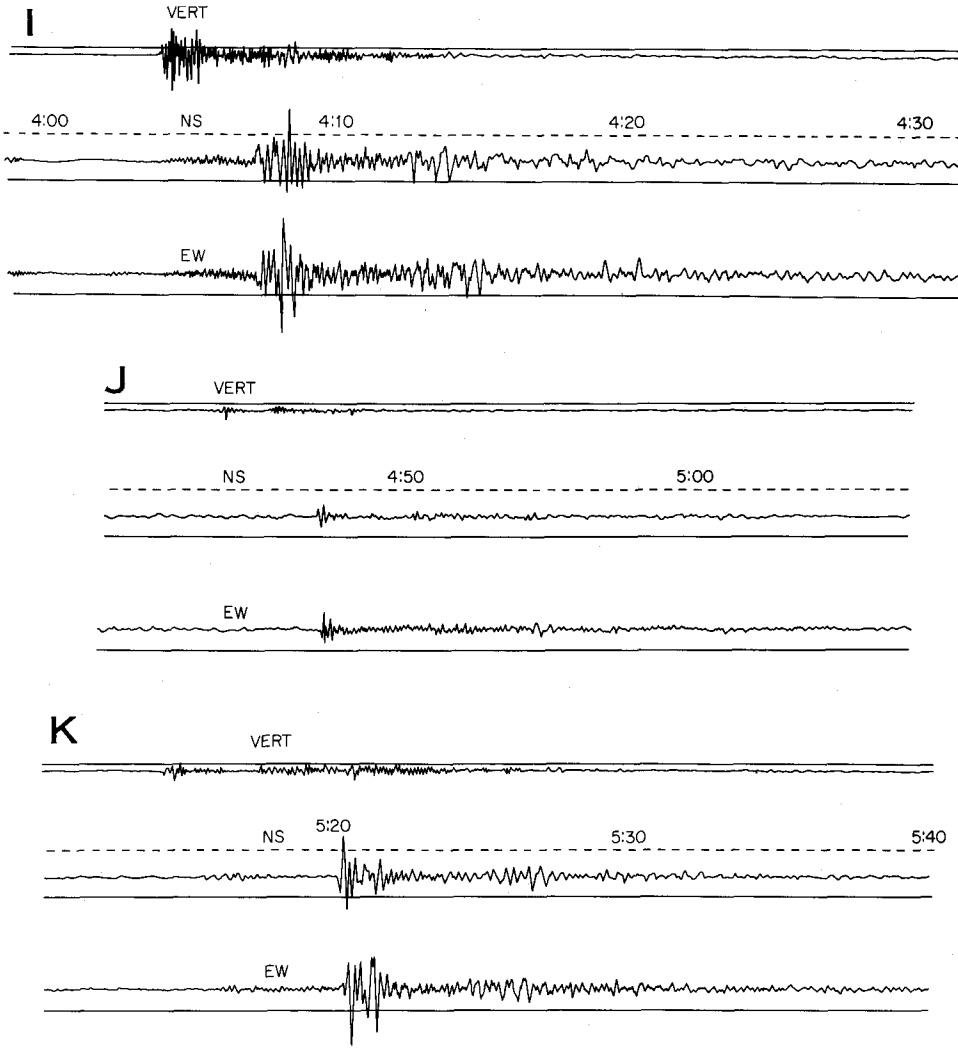

FIG. 2i. El Centro strong motion accelerograph record for event 9.
FIG. 2j. El Centro strong motion accelerograph record for event 10.
FIG. 2k. El Centro strong motion accelerograph record for event 11.

a distance correction for amplitudes is made (distance is estimated from the S-P times) it is found that the magnitudes of some of these later events are only about 0.6 to 0.9 magnitude units less than the largest event (event 2), and are thus important in earthquake engineering studies.

Because of large amplitudes, high frequency oscillations, and trace overlap, the original El Centro strong motion record (Figure 2a) is confusing. To improve readability of this record all three traces were digitized and replotted at reduced gain in Figure 2b. Although this record appears complicated, when it is compared with aftershock events

(e.g., event 9 in Figure 2i), similar wave forms can be recognized. Higher frequency phases on EW and NS components represent S waves from the more or less distinct events. At least four S arrivals corresponding to events designated 1A, 1B, 1C, and 2 can be seen in Figure 2b. Corresponding P-wave arrivals for each of these events cannot be unequivocally identified because of the constant high level of the short period pulsations caused by all preceding events. Probable P-wave arrivals for these events are indicated in Figure 2b by an arrow.

In order to interpret the phases recorded in Figure 2a to Figure 2k, travel-time curves and dispersion curves were constructed from a five layer model of the Imperial Valley (Westmoreland profile, after Biehler, 1964). The travel-time curves were used to estimate the distance of each event. To compute the surface wave dispersion curves, layer thicknesses, velocities, and densities were assumed as follows:

Layer	*thickness (km)*	α *(km/sec)*	β *(km/sec)*	ρ *gr/cm*^{3}
1	.18	1.70	.98	1.28
2	.55	1.96	1.13	1.36
3	.98	2.71	1.57	1.59
4	1.19	3.76	2.17	1.91
5	2.68	4.69	2.71	2.19
6	∞	6.40	3.70	2.71

Poisson's constant was taken to be $\frac{1}{4}$. Densities in the last column were calculated using the empirical relationship of Birch (1961)

$$\rho = 0.770 + 0.302\ \alpha.$$

The shallow densities calculated in this way are adequate for the dispersion analysis in this paper but are not realistic for actual surface layers.

Dispersion curves calculated for this model (Figure 3) show the group velocities for the first four Love and Rayleigh modes. The flat character of the fundamental mode curves indicate that most of the energy in the period range 0.5 to 5.0 seconds will travel with a velocity of about 1 km/sec.

The epicentral distances of each event were determined from the P- and S-wave arrival times on the El Centro strong motion seismogram. These distances were checked against the surface wave arrival times. Using only arrival times at one station it is not possible to determine the position of each event, however, if we assume that all events occurred along the observed surface trace of the fault southeast of El Centro, it is then possible to locate the relative position of these events along this surface trace. The assumption that the epicenters of all events lie along the surface trace of the fault to the southeast cannot be strictly justified, but appears to be a reasonable first approximation. Certainly the locus of the main energy release events must be near the observed fault trace. Aftershocks of large earthquakes also usually cluster around the fault rupture, and some recent studies of precisely located aftershocks indicate that most of the events lie very close to the fault trace (Parkfield earthquake, 1966, Eaton, 1967; Borrego Mountain earthquake, 1968; Hamilton and Healy, 1969). The fact that the observed fault offset (Figure 9) increased towards the southeast and that the biggest displacements were recorded close to the international boundary suggests that most of the energy release took place SE of El Centro. The main energy release and fault rupture appears to be represented by the first 25 seconds of the strong motion record (Figure 2a). As mentioned earlier, the identification of P-wave arrivals for the 4 events on this

section of the record is rather uncertain because the P waves are less pulse-like than the S wave and variable in relative amplitude (e.g., compare the various events in Figures 2c to 2k). Because of the complexity of this section of the record several other smaller events could have occurred and not been identified. The longer period pulses on the NS and EW components arriving at about 4 and 11 seconds are probably surface waves corresponding to events 1A and 1B, respectively. The excitation of 2 cps surface waves is variable, in some cases a prominent surface wave pulse is observed and in other cases not (Figures 2b to 2k). This variability is probably related to variations in the depth of the events. The S wave for event 2, probably the largest event of the series, arrived some 24 seconds after the first event. The P-wave time and therefore the distance of this event is somewhat uncertain but is probably as indicated in Figure 2b, which

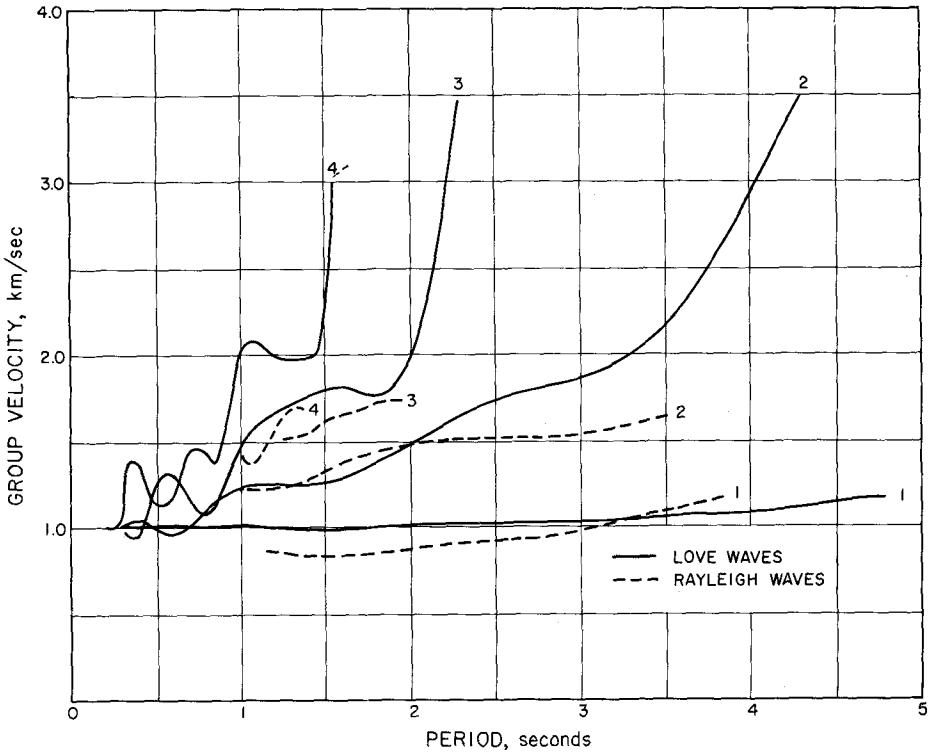

FIG. 3. Love and Rayleigh wave dispersion curves for the structure corresponding to the Westmoreland profile (Biehler, 1964) in the Imperial Valley.

would place the event at the southeasternmost part of the break, similar to event 6 (Figure 2f) and event 11 (Figure 2k). We interpret the El Centro strong motion record to indicate that the main fault rupture occurred along a section of the fault from near the initial epicenter southeast to near Cocapah in a series of more or less discrete events which occurred in a time span of about 15 seconds and are represented on the first 25 seconds of the record.

Event 2 might be called a "stopping phase" in the sense that it probably represents the last event in a series of events successively further toward the southeast, but probably does not represent a stopping phase in the idealized sense for perfect interference as described by Savage (1965).

We have assigned magnitudes to the various events using the definition of local earth-

quake magnitude (Richter, 1958). The strong motion record (Figure 2a to 2k) was used to calculate the response of a Wood-Anderson type instrument with the following constants: $V_s = 2800$, $T = .8$ sec, and $\zeta = 1.0$. Magnitudes $M_L^{S.M.}$ measured in this way should be the same as determined on a Wood-Anderson instrument at El Centro, and are given in Table 1.

TABLE 1

MAGNITUDES FOR EVENTS IN THE IMPERIAL VALLEY EARTHQUAKE OF 1940

Event	Distance (km)	$M_L^{S.M.}$*	M_L†
1A	7–15 ?	5.9–6.1	—
1B	17–23 ?	6.0–6.2	—
1C	13–19 ?	5.7–5.8	—
2	35–44 ?	6.4–6.6	6.4
3	20–28	4.8–5.1	—
4	13–19	4.3–4.5	—
5	8–12	4.4	—
6	34–43	5.3–5.5	—
7	25–34	4.6–5.0	—
8	24–32	4.3–4.6	—
9	13–19	5.1–5.2	5.2
10	14–20	4.6–4.7	—
11	33–43	5.8–5.9	4.8

* Calculated from computed response of the Wood-Anderson instrument at El Centro.
† Calculated from distant stations (Table 2).

TABLE 2

DATA USED IN DETERMINING THE LOCAL MAGNITUDE M_L FOR THE IMPERIAL VALLEY EARTHQUAKE OF 1940

Station	Direction	Distance (km)	Distance Correction	Station Correction	Max $A_{(mm)}$	Log A	M
Tinemaha	EW	546	4.8	−.2	51	1.70	6.3
	NS				79	1.90	6.5
Haiwee	EW	440	4.6	0.	110	2.04	6.6
	NS				141*	2.10	6.7
Riverside	EW	224	3.7	+.2	188*	2.30	6.2
	NS				—	—	—
Mt. Wilson	EW	290	4.0	—	143	2.16	6.2
	NS				181*	2.26	6.3
Pasadena	EW	294	4.0	+.2	125*	2.10	6.3
	NS				160*	2.20	6.4
Santa Barbara	EW	435	4.6	−.2	140*	2.15	6.5
	NS				153*	2.18	6.6

* Peak deflections off scale were estimated by extrapolation.

The local magnitude of $M_L = 6.4$ for the main shock was determined by taking the grand average from EW and NS components of the Wood-Anderson seismograph records at Tinemaha, Haiwee, Mt. Wilson, Pasadena, and Santa Barbara, and EW component at Riverside (see Table 2) and agrees with the local magnitude derived from the strong motion instrument. Magnitudes $M_L = 5.2$ for event 9, and $M_L = 4.8$ for event 11 were computed from the EW and NS records from Mt. Wilson and the EW component from Riverside. M_L for event 9 agrees closely with the determination from the

strong motion instrument, however, event 11 gives a magnitude 1 unit higher on the strong motion instrument than on Wood-Anderson instruments at large distances. The spectrum of this event is obviously much different than that of event 9. Note especially that the P wave for this event contains hardly any of the high frequency (5–10 cps) energy obvious in the other aftershocks. The relatively great excitation of high frequencies for event 9, suggests that it may have been deeper than events 6 and 11, assuming that deeper shocks occur under higher stress and thus generate higher frequencies. If this interpretation is correct it would explain the difference between $M_L^{\text{S.M.}} = 5.8$–5.9 and $M_L = 4.8$ for event 11. In addition, the change of amplitudes with distance is strongly dependent on the uncertain depth of the source at these close distances.

Analysis of Distant Records

Fourier Spectrum, $F(\omega, t^*, \Delta t)$, of the Tinemaha Records. In a simple Fourier analysis of the complete complex record, information on the time dependence of the incoming wave forms, i.e., the time of their arrivals, duration, and dispersion properties are not directly displayed. Therefore, we use the following form of moving window Fourier analysis:

$$F(\omega, t^*, \Delta t) = \int_{-\infty}^{\infty} e^{-i\omega t} f^*_{\Delta t}(t)\, dt$$

where

$$f^*_{\Delta}(t) = \begin{cases} 0; & t \leqq t^* - \dfrac{\Delta t}{2} \\ f(t)a(t); & t^* - \dfrac{\Delta t}{2} \leqq t \leqq t^* + \dfrac{\Delta t}{2} \\ 0; & t \geqq t^* + \dfrac{\Delta t}{2} \end{cases}$$

and $f(t)$ stands for the record trace as a function of the time. This formulation is equivalent to taking the Fourier amplitude spectrum of the function $f(t)$ multiplied by the window of the form:

$$W_{\Delta t}(t^*) = \begin{cases} 0; & t \leqq t^* - \dfrac{\Delta t}{2} \\ a(t); & t^* - \dfrac{\Delta t}{2} \leqq t \leqq t^* + \dfrac{\Delta t}{2} \\ 0; & t \geqq t^* + \dfrac{\Delta t}{2} \end{cases}$$

so that

$$f^*_{\Delta t}(t) = f(t) W_{\Delta t}(t^*).$$

It is evident that $F(\omega, t^*, \Delta t)$ can be used for several purposes. For example, if the time coordinate t^* is taken as the travel time, then for a given distance, $F(\omega, t^*, \Delta t)$ yields the dispersion properties of the incoming waves. In addition, for complicated

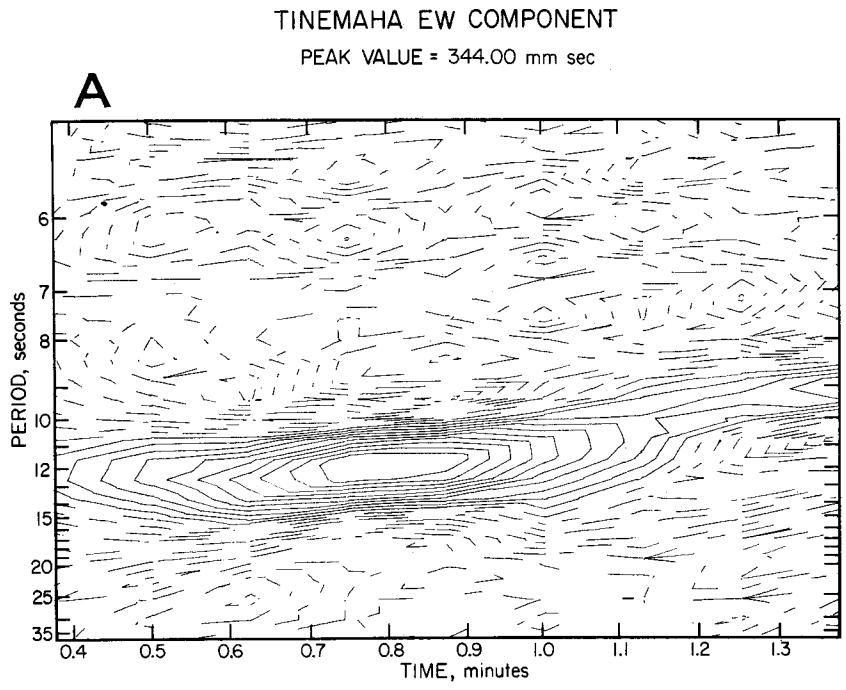

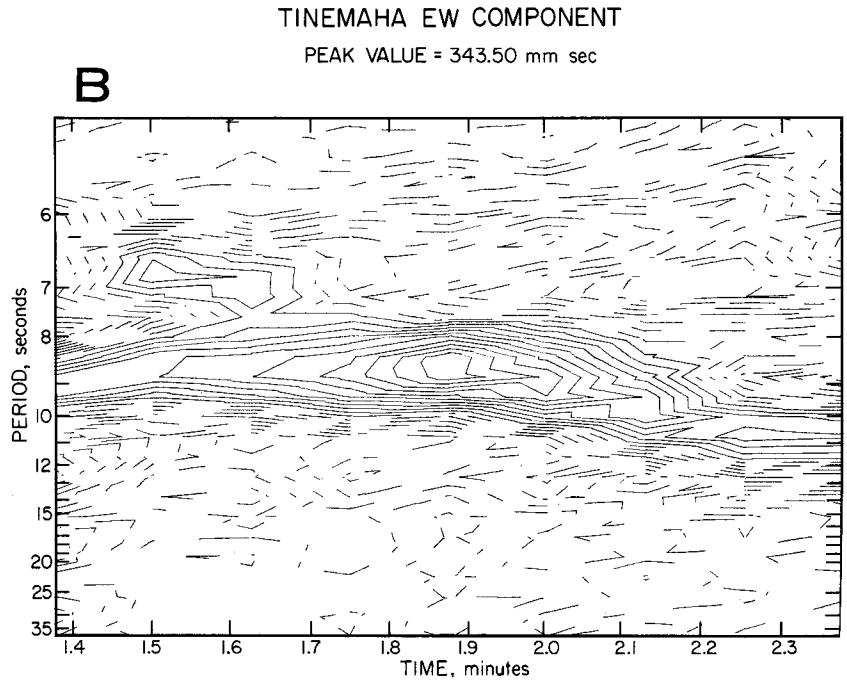

FIG. 4a. Moving window Fourier spectrum $F(\omega, t^*, \Delta t)$ for the Tinemaha seismogram of the Imperial Valley earthquake of 1940.

FIG. 4b. Moving window Fourier spectrum $F(\omega, t^*, \Delta t)$ for the Tinemaha seismogram of the Imperial Valley earthquake of 1940.

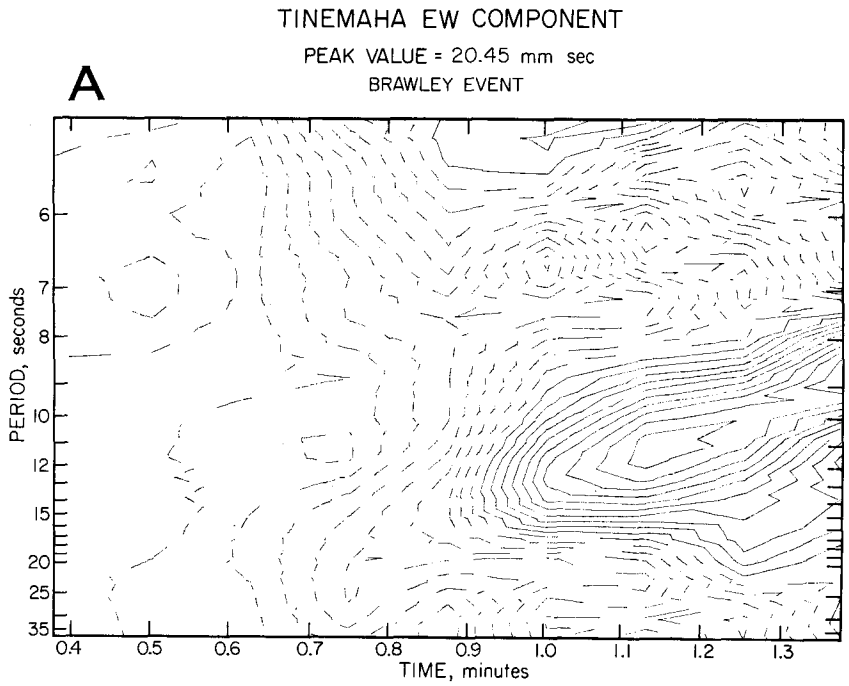

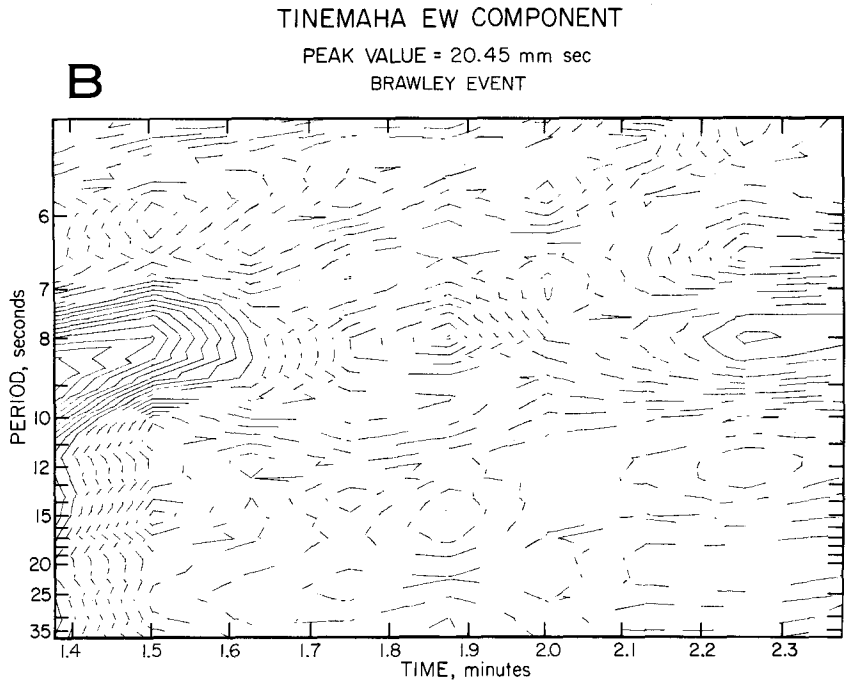

FIG. 5a. Moving window Fourier spectrum $F(\omega, t^*, \Delta t)$ for the EW seismogram of the Brawley event recorded at Tinemaha.

FIG. 5b. Moving window Fourier spectrum $F(\omega, t^*, \Delta r)$ for the EW seismogram of the Brawley event recorded at Tinemaha.

records, in particular, records of multiple event earthquakes, $F(\omega, t^*, \Delta t)$ can be used to separate different events or different phases. The choice of Δt, i.e., the window width (as well as the window shape), depends on the particular needs of the analysis, and has to be chosen in each case to suit the physical character of the function $f(t)$ to be analyzed.

In this work only a square window, $a(t) = 1.0$, is used. To analyze the record $f(t)$, a discrete set of ω_i, $i = 1, 2, \cdots, n$ and t_j^*, $j = 1, 2, \cdots, m$, together with Δt are chosen. If ω_i are chosen, $F(\omega_i, t_j^*, \Delta t)_{i=1,\cdots,n;\ j=1,\cdots,m}$ for n and m large enough, will approximate a continuous function $F(\omega, t^*, \Delta t)$. We have used equally spaced ω_i's and

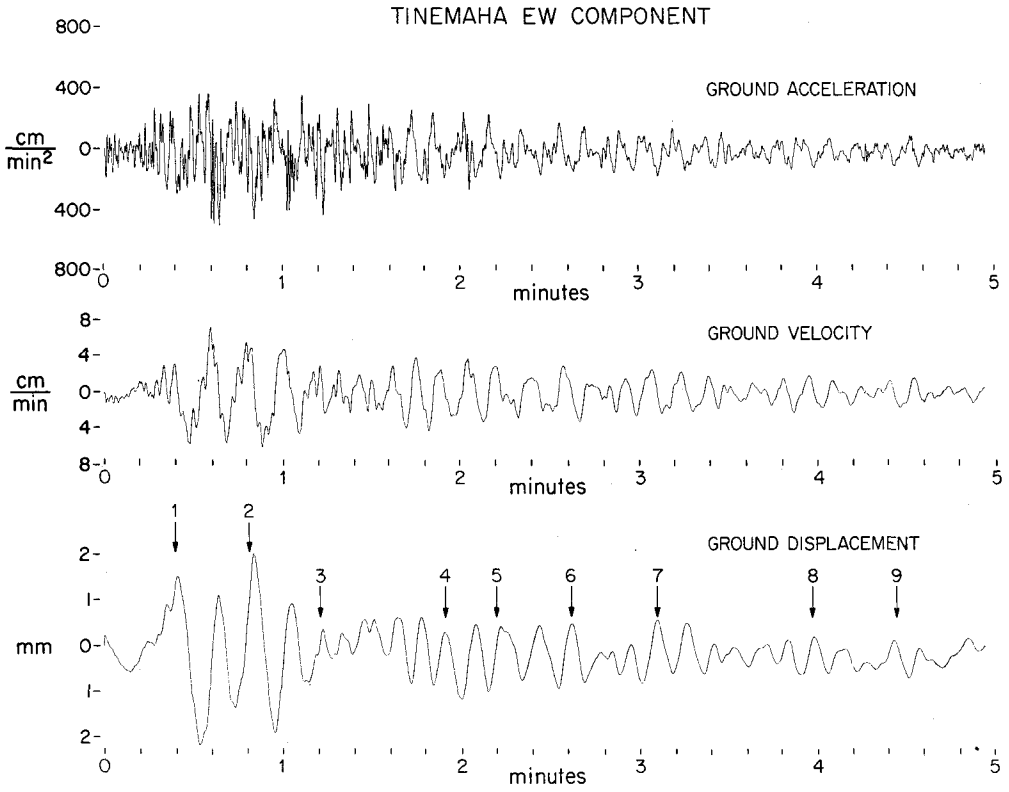

FIG. 6. Calculated EW ground acceleration, velocity and displacements at Tinemaha for the Imperial Valley earthquake, 1940. Arrows indicate expected arrival times for events as inferred from the El Centro strong motion seismogram.

t_j^*'s and linearly interpolated $F(\omega, t^*, \Delta t)$ between the discrete points. The records were digitized using a Benson-Lehner data reducer and the spectrum calculated on an IBM 7094. Several Δt intervals were used during the course of the work in order to study the properties of $F(\omega, t^*, \Delta t)$. The final window width was chosen to be $\Delta t = .75$ min and increments in t^* were taken as $\frac{1}{8}$ min. $F(\omega, t^*, \Delta t)$ was plotted using a Calcomp plotter (Figures 4a to 5b). Each plot represents $F(\omega_i, t_j^*, \Delta t)_{i=1,\cdots,n;\ j=1,\cdots,m}$ for an interval of one minute and for the frequency range from 10 to 75 rad/min (periods 35 to 5 sec). All plots were normalized, each with respect to the maximum peak value that occurred in that 1 min time interval, so that spectral values range from 0.0 to 1.0 of that peak value. The interval from 0.0 to 1.0 was subdivided into 20 levels. Levels of value greater than 0.5 were connected with full contour lines in order to clearly display the peaks in the spectrum.

Figures 4a and 4b give the spectra obtained for the EW component at Tinemaha. The spectra are not corrected for the instrument response; however, such correction would not critically alter their appearance. Time on these figures corresponds to the time on Figure 6 and is measured in minutes from an arbitrary point at which the record digitization was initiated.

An aftershock, herein called the Brawley event (Figure 7, 19 May 1940, 5:51 GCT, $M = 5.5$), was used as an example of a simple event and the spectrum was computed and plotted (Figures 5a and 5b) in the same manner as for the main event. As can be seen in Figure 5a and Figure 5b the spectrum corresponds to a slightly dispersed train of waves lasting for about $\frac{1}{2}$ min with predominant periods between 7 and 20 seconds.

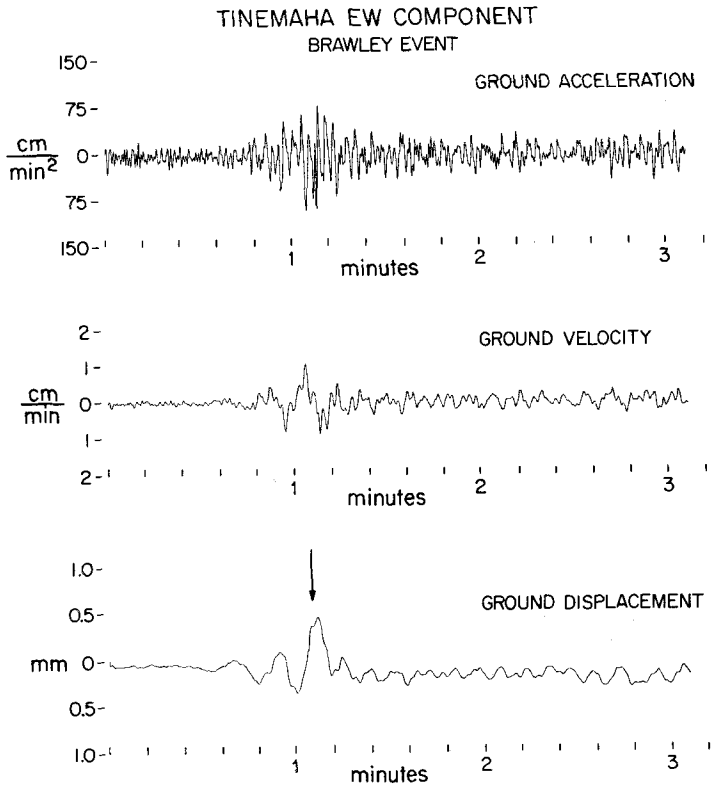

FIG. 7. Calculated EW ground acceleration, velocity, and displacements for the Brawley (19 May 1940, 5:51 GCT) event recorded at Tinemaha.

A similar analysis made for a recording from the Haiwee Wood-Anderson instrument showed essentially the same features. The locations of Tinemaha ($\theta = 8°$) and Haiwee ($\theta = 4°$) are such that EW motion represents essentially pure Love waves.

Integrated and Filtered Distant Records. The Tinemaha EW components of the Wood-Anderson records of both the Brawley event (Figure 7) and the main sequence (Figure 6) were corrected to give true ground acceleration as a function of time. The instrument constants used for the instrument correction were: $V_s = 2800$, $T = .8$ sec, and $\zeta = 1.0$. The corrected ground motion was then high pass filtered to eliminate periods greater than approximately 30 sec. This was done because of possible uncertainties resulting from the data processing procedures and the large instrumental correction necessary.

The Wood-Anderson torsion seismograms at Tinemaha, Haiwee, Mt. Wilson, and Riverside were also analyzed as a group using a simple running mean low-pass filter

in order to find whether there has been a coherent pattern to the waves in the coda at these stations. The corner period on the filter was about 15 seconds. Low-pass filter records from these four stations together with the EW record from a long-period torsion instrument at Pasadena are plotted in Figure 8.

Interpretation of Distant Records. Comparison of the Fourier amplitude spectra for the Brawley event (Figures 5a and 5b) and the main sequence (Figures 4a and 4b) or a comparison of the calculated ground motion on Figures 6 and 7 illustrates the complexity of the main earthquake. If all the source parameters associated with each of the multiple events were similar to the Brawley event and if there were sufficient time intervals between each two successive events so that interference would be negligible, it would be possible to identify all individual events on a long-period ground motion record such as in Figure 6 by simply identifying a "characteristic" peak (e.g., indicated by an arrow in Figure 7). However, this is not the case for the Tinemaha record of the

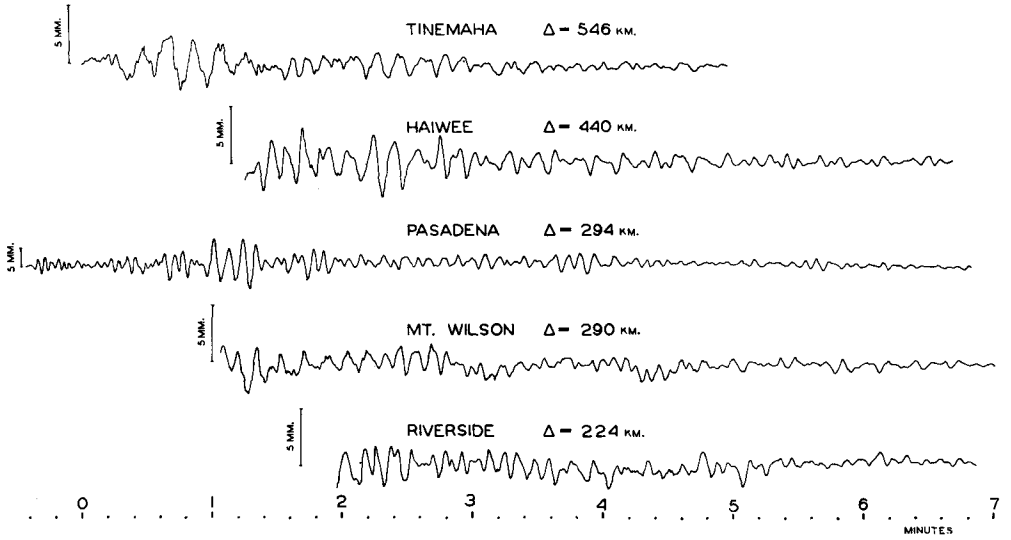

FIG. 8. Surface waves from Imperial Valley earthquake, California, 1940 recorded on low-pass filtered EW seismograms from Wood-Anderson instrument at Tinemaha, Haiwee, Mt. Wilson, and Riverside, and on the low magnification long-period record from Pasadena.

Imperial Valley Earthquake. As can be seen from the calculated ground motion (Figures 6 and 7) and Fourier spectra (Figures 4a and 4b) the predominant period of waves recorded at Tinemaha was about 10 seconds. The duration of the surface wave train for a single event, e.g., the Brawley event is about 30 seconds or 3 cycles of about a ten second period wave. This makes it difficult to resolve events separated by less than 30 seconds. Arrows numbered 1 to 9 in Figure 6, are spaced to represent the relative arrival times predicted at Tinemaha. The arrows on the basis of the approximate locations indicated by numbers 1A, 1B, $\cdots$, 11 in Figure 1a have been time shifted as a group to give the best agreement with the first pulse of energy. Number 1 in Figure 6 stands for the group of events 1A, 1B, and 1C, on the strong motion record.

Because of the close spacing of events 1A through 2, they cannot be resolved by the long-period ($\sim$10 sec) surface waves recorded at Tinemaha. These waves thus combine to give approximately the effect of a source propagating to the southeast. The shape of the Fourier spectra corresponding to these events (Figures 4a and 4b) is consistent with this interpretation as is the Tinemaha ground motion record which can be

explained as a superposition of several pulses shaped like the single pulse from the Brawley event. This interpretation is also supported by the difference of .7 on the Richter magnitude scale, between the local stations (M_L = 6.4) located mainly NW from El Centro and teleseismic stations (M_S = 7.1) located E and SE, suggesting independently that during the main energy release the source propagated toward the SE.

Local magnitudes $M_L^{S.M.}$, estimated above from the strong motion record at El Centro suggest that events 3, 6, 7, 9, and 11 might have been large enough to generate significant long-period energy. The prolonged train of surface waves on the EW component of ground motion at the Tinemaha station (Figure 6) show long-period ($\sim$10 sec) wave arrivals which might be associated with these events. However, filtered records from other local stations (Haiwee, Mt. Wilson, Pasadena, Riverside) show no coherent pattern associated with these events. This suggests that the prolonged train of surface waves consists of scattered reflections from crustal inhomogeneities that have been generated by the main events (first 15 seconds) but travelled indirect reflected paths to the seismograph station. Figure 8 gives low-pass filtered records (corner period approximately 15 sec) from these stations, time shifted according to distance so that a surface wave travelling with a velocity of 3.5 km/sec arrives at the same time on all records. Although there is no coherent pattern, it is obvious that the "coda" of surface waves is longer and more complex than that following the Brawley (single-event) earthquake. This may have, in part, resulted from the greater relative excitation of long-period surface waves by the main events since the "coda" consists of primarily longer period waves. It is quite possible that the largest of these events (e.g., nos. 6, 9, and 11) generated surface waves that could have been clearly observed if it had not been for the large amplitudes of the scattered surface waves from the first part of the rupture. The magnitudes of these events were unusually large for ordinary aftershocks. According to the Båth's law (Richter, 1958) the magnitude of the largest aftershock is usually about 1.2 less than the main event. Thus, although the main energy release during this earthquake probably occurred in the first 15 seconds, significant energy release occurred as late as event 11 some 5 minutes later. It is also possible that significant long-period energy continued to be radiated after the first 15 seconds in some complex manner not simply related to the inferred magnitudes of events 2 to 11. That there may be considerable variation in the ratio of long-period to short-period excitation is indicated by an inspection of the various aftershocks, in particular, events 9 and 11.

Field Observations of Fault Offset

Figure 9 shows the amount of right lateral offset along the Imperial fault as it was observed in the field shortly after the May 19, 1940 earthquake (Buwalda, unpublished field notes). The pattern of these offsets indicates that the main part of the displacements took place along a surface fracture some 20 to 25 km long extending approximately from the instrumentally determined epicenter of the main shock SE some 5 km past Cocopah (Figure 1a). Tentative location of the main sequence of events 1A, 1B, 1C, and 2 (Figure 1a) or an "equivalent" propagating rupture towards SE along the same section of the fault, are in agreement with the observed surface displacement (Figure 9). In addition, the distribution of the set of 9 aftershocks (Figure 1a) supports the conclusion that the main energy release took place along the same 20 to 25 km section of the fault. The observed fault offset (Figure 9) NW of the instrumentally determined epicenter (Figure 1a) is probably associated with the Braw-

ley event, as suggested by Richter (1958). Repeated surveying of the Imperial fault since 1940 indicates (Brune and Allen, 1967) that there has been creep along the northwestern part of the fault trace. On March 4, 1966 there was a low-magnitude earthquake (M = 3.6) with surface faulting along 10 km of the fault trace, centered about the point nearest to the El Centro, the same northwestern part of the Imperial fault which was fractured during the 1940 sequence (Brune and Allen, 1967). The 1963–1967 California Institute of Technology Local Bulletin of Earthquakes indicate several events in the magnitude 3.0 to 4.9 along the northern section of the fault, but none on the SE section of the fault. The Borrego Mountain, California, earthquake of 9 April 1968 (M = 6.5) triggered creep episodes on several fault systems including the Imperial fault. Theodolite resurveys (Allen *et al.*, 1968) indicate, 1.2 cm cumulative right lateral displacement at the point where highway 80 crosses the Imperial

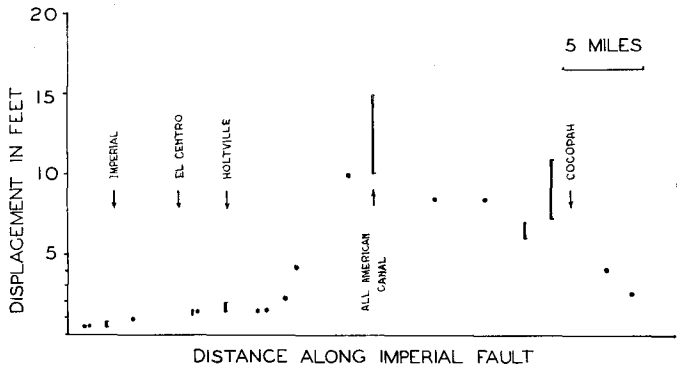

FIG. 9. Plot of the relative displacements along the fault trace as measured in the field by J. P. Buwalda (original notebook and some additional data were kindly supplied by Prof. C. R. Allen). Vertical lines indicate the range of the observed displacements at essentially the same locality.

fault (Figure 1a), 1.1 cm 6 km northwest, and 1.3 cm 11 km northwest from the same locality. These new triggered breaks along the Imperial fault extended for more than 20 km in the same region as the small earthquake of 1966 (Brune and Allen, 1967). Allen, Brune and Lomnitz (personal communication) did not find any evidence of recent fault slippage at either the locality of the All American Canal (Figure 1a) or in the vicinity of Cocopah as of January, 1969. The recent activity along the northwestern part of the Imperial fault suggests that it is behaving at present differently than the section southeast of the epicenter of the 1940 earthquake. This difference could perhaps be related to the fact that the NW part of the fault did not slip as much as the SE section of the fault during the May 19, 1940 earthquake, but was rather fractured by the later aftershock activity, fault creep or both, and remained in a higher state of strain.

Computation of Source Moment Using Seismic Waves

Seismic moment was calculated using relations from Ben-Menahem and Harkrider (1964) for a vertical strike-slip surface fault and including a correction for directivity function; i.e.,

$$M_0 = \frac{u_\theta^{dc}}{A_L \cos 2\theta} \cdot \sqrt{2\pi\Delta C\omega} \cdot \left| \frac{\chi}{\sin \chi} \right|$$

where

$$\chi = \frac{\pi b}{CT_0}\left(\frac{C}{v} - \cos\theta\right)$$

To take into account the attenuation of the waves due to scattering and anelasticity (together with other sources of the energy loss), and to correct for the angle δ of the EW component relative to the u_θ^{dc} direction, we write for u_θ^{dc}:

$$u_\theta^{dc} = ue^{\pi\Delta/QUT_0}\frac{1}{\cos\delta}$$

where u is the spectral density determined from the record.

In the case of a multiple event earthquake where the individual events are sufficiently separated in time, the moment may be calculated as the sum of the moments associated with each event. If we denote each such moment by $M^i_{0\text{-SEISM}}$, then

$$M^{\text{TOT}}_{0\text{-SEISM}} = \sum_i M^i_{0\text{-SEISM}}$$

The sequence of 4 events that occurred in the first 25 seconds on the onset of the strong motion record were too closely spaced for this condition to apply to the waves of about 10 seconds period recorded at Tinemaha. For these waves the multiple events behave more like a propagating source.

To correct for directivity it is necessary to know the rupture length and the propagation velocity. From the plot of displacements (Figure 9) and the distribution of aftershocks shown in Figure 1a, the main rupture appears to have extended from the epicenter to Cocopah, a distance of about 20 to 25 km. The rupture velocity is approximately given by the fault length divided by the time difference between the triggering of the strong motion instrument and the origin time of the last event, about 15 seconds. This gives an effective rupture velocity of about 2 km/sec. Estimates of the source parameters (b = 20–25 km, $v \approx 2$ km/sec, $C \approx 3.4$ km/sec at T_0 = 11 sec, and $\cos\theta = -.99$) give an approximate value for χ to be 4.5 to 4.0 and $|\sin\chi/\chi| \sim .20$ which is in approximate agreement with the shape of the spectrum given in Figure 4a, as indicated by spectral gaps at periods of about 9 and 15 seconds. With the above assumptions we obtain

$$\text{at Tinemaha:} \quad M_{0\text{-SEISM}} \approx 1.1 * 10^{26} \text{ dyne-cm}$$

$$\text{at Haiwee:} \quad M_{0\text{-SEISM}} \approx 1.3 * 10^{26} \text{ dyne-cm.}$$

In these calculations the following values were used: $Q \approx 200$; $A_L = .91 * 10^{-18}$ cm/dyne; T_0 = 11 sec; $R_{T_0=11}$ = ground amplitude in microns/trace amplitude in millimeters = 60; C = 3.7 km/sec; Δ = 546 km for Tinemaha; Δ = 440 km for Haiwee; $\delta_{\text{HAIWEE}} = 31°$; $\delta_{\text{TINEM.}} = 27°$. These two determinations are considered to be in good agreement considering the difficulty in the interpretation and the accuracy of the necessary assumptions.

Computation of Moment from Field Observations

The computation of the moment from field observations was performed using the well known relation (Maruyama, 1963; Aki, 1966; Brune and Allen, 1967):

$$M_{0\text{-FIELD}} = \bar{u}\mu A$$

From the field evidence the average displacement along the complete fault length measured on the surface of the ground was 1.25 m. The fault length was about 65 km (Richter, 1958). The depth of the faulting was estimated to be about 7 km by fitting the geodetic data given by Byerly and DeNoyer (1958) with the theoretical curve for a strike-slip fault taken from Knopoff (1958). With $\mu = 3.3 \times 10^{11}$ dyne/cm^2, one obtains for the whole fault plane

$$M_{0\text{-FIELD}} = \tfrac{3}{4} * 1.25 * 3.3 * .7 * 6.5 * 10^{25} = 1.4 * 10^{26} \text{ dyne-cm.}$$

However, if the northwestern section of the fault did not slip during the main event, but later during the Brawley event as suggested above, then the field moment for the main event should be calculated from the southern section only.

Taking the length of the fault section corresponding to the main propagating rupture to be about 25 km fault depth of 7 km and the average displacement of 2.7 meters corresponding to the fault section between the All American Canal and Cocopah, one obtains essentially the same moment.

$$M_{0\text{-FIELD}} = \tfrac{3}{4} * 2.7 * 3.3 * .7 * 2.5 * 10^{25} = 1.2 * 10^{26} \text{ dyne-cm}$$

We may expect the moment estimated from the field evidence to be somewhat larger than that estimated from the seismic results because the field observations include fault slippage occurring during later aftershocks as well as creep. Considering the uncertainties involved in both the field data and the seismic analysis, the agreement is remarkable.

Magnitude and Moment

The published magnitude for the Imperial Valley earthquake of 1940 is 6.7 (Richter, 1958). However, a strictly objective determination of magnitude using Wood-Anderson torsion seismometer records gives a value of 6.4. The magnitude indicated from the strong motion instrument is about 6.5. It was originally felt that more weight should be given to distant stations in the assignment of 6.7 as the magnitude. The magnitude M_L* = 6.4 is obtained from the average of magnitudes determined using maximum deflections on EW and NS Wood-Anderson components at stations Tinemaha, Haiwee, Mt. Wilson, Pasadena, Santa Barbara, and Riverside as shown in Table 2. The period of these deflections is about 1 sec.

Subsequently, Gutenberg increased the magnitude to 7.1 on the basis of determinations of 20 second surface wave magnitudes for stations La Plata, Uppsala, DeBilt, Stuttgart, and Helwan† and body wave magnitude (using *PH*, *PPH*, and *S*) at La Plata. The higher magnitude was considered to be in better agreement with field evidence of extensive faulting.

In the case of multiple event earthquakes, obviously the magnitude versus moment relationship need not be single valued since an increase in the number of events will in-

* By definition, $M_L = \log A - \log A_0$ where A is the amplitude in mm of the trace recorded by a standard Wood-Anderson torsion seismometer ($V = 2800$, $T = .8$ sec., $\zeta = .8$) at a distance of 100 km from the epicenter, and A_0 is the amplitude with which the same instrument would record an earthquake of magnitude zero, at this distance. The magnitude defined in this way is a measure of the largest amplitude of ground motion at a given distance. Determination of magnitude in this manner is not considered reliable at distances greater than about 600 km.

† Professor C. F. Richter kindly helped us in finding and interpreting the original notes written by Professor B. Gutenberg.

crease the total moment but not necessarily the maximum amplitude. Thus an earthquake of magnitude say 8.4, determined from long-period waves would not generate 100 times greater accelerations than those observed for the Imperial Valley earthquake with $M_L = 6.4$. The magnitude calculated from the moment (long-period waves) will tend to be larger than the magnitude determined from the record of the short-period waves. The magnitude directly determined from the record of the short-period waves will correspond more closely to the moment for the single event which generated the biggest short-period waves. Stated otherwise, a series of events propagating in space will constructively interfere for wavelengths large compared to the source dimensions, but not constructively interfere for shorter wavelengths (Brune and King, 1967).

Destructiveness of Multiple Event Sources

As can be seen in Figures 2a to 2k at least 13 events occurred in the period of approximately 6 minutes, one large event every 5 to 10 seconds during the first 25 seconds and about one clearly recorded event every 25 to 30 seconds during the next 5 minutes. The shortest resolved time interval between two distinct events was close to 4 seconds and the longest 50 seconds. However, other events not resolved could have occurred at shorter intervals. The interval between relatively large events during the latter 5 minutes was of the order of 1 minute.

The effect of a given ground motion on typical engineering structures is commonly investigated by calculating the response spectrum. This has been done in the engineering literature for the first 30 seconds of the Imperial Valley, 1940 earthquake; including the first four events (Alford *et al.*, 1951). It is now of interest to investigate the additional effects on structures that might be associated with the later events.

If the building is represented by a one degree of the freedom simple oscillator with a natural circular frequency of vibration p and a fraction of critical camping ζ, the transient response to a given initial velocity and displacement is

$$x = e^{-p\zeta t}[c_1 \sin p\sqrt{1 - \zeta^2}\, t + c_2 \cos p\sqrt{1 - \zeta^2}\, t]$$

where c_1 and c_2 depend on the initial velocity and displacement. This is an oscillatory motion with the amplitude given by

$$A(t) = e^{-p\zeta t}.$$

Many buildings have a small equivalent viscous damping, not exceeding 2 percent if vibration is in the elastic range of perhaps 5 percent to 8 percent if the vibration level is in the plastic range. The natural period of the vibration of most buildings would fall in the range from $T = .05$ sec, for small stiff structures to $T = 4.0$ sec or greater for tall and flexible structures.

If we suppose that the excitation of the building vibration is small between the successively arriving events, the vibration will die out during the "quiet" interval of time as $e^{-p\zeta t}$. When $p\zeta t$ becomes close to 3.0 the amplitude of the oscillatory motion will be 20 times smaller than at the beginning of the quiet interval ($t = 0$), i.e., at the moment when the excitation caused by the nth event has just ceased to be signifidant. This qualitative argument gives

$$t_{1/20} = \frac{3}{\zeta p} \quad \text{or} \quad t_{1/20} = \frac{3}{2\pi}\frac{T}{\zeta}.$$

If we take $T = 1.0$ sec and $\zeta = .02$ we get $t_{1/20} = 24$ sec. Thus for most cases of buildings excited by a sequence of events similar to the Imperial Valley earthquake, the vibration will nearly die out between most of the individual events. Buildings with relatively short natural periods of vibration (say 1 sec or smaller) will respond to a sequence of the events such as the Imperial Valley earthquake, as if there were 13 or more different earthquakes each with duration of 3 to 30 sec. For such buildings the time build up of the amplitude of the vibration will depend on the duration of each single event and the occurrence of a new event every 30 sec or so will not be important for response amplitude, although it might be important if progressive weakening is involved.

For buildings whose natural period of vibration is longer, amplitudes may be cumulatively increased by the sequence of events. The actual rate at which building vibrations grow will depend on the effects of the interference of the waves coming from the successive events, on the number and duration of events, on the distance between the structure and each event, and on the elapsed time between events. It is clear that for a sequence of events with similar long-period wave amplitudes, the response amplitude could increase with the total number of the events in the multiple sequence. In this case, there might well be a good correlation between destructiveness and seismic moment (or equivalently to the amplitudes of very long-period waves, e.g., mantle wave magnitude, Brune and Engen, 1969).

Presently, there are increasing numbers of tall buildings and other structures with long natural periods of vibration which may be subject to vibration with cumulatively increasing amplitudes if excited by a sequence of events similar in character to the Imperial Valley earthquake of 1940. In order to accumulate necessary data for analysis of such structures calculation of the relative velocity spectra should be extended to longer natural periods of vibration, say up to 10 sec. In addition, much longer portions of the available strong motion accelerogram records should be used as an input for their calculations in order to allow for the build up of the oscillation amplitudes.

Conclusions

(1) Analysis of the P, S, and short-period surface waves recorded on the El Centro strong motion accelerometer indicates that the Imperial Valley earthquake of May 19, 1940, consisted of a series of at least 13 distinct events occurring during the period of about 6 minutes and distributed over a distance of about 25 km SE along the fault from the initial epicenter. Most of the energy and seismic moment was produced in the main sequence of about 4 events which occurred in the first 15 seconds and were distributed over the same section of the fault. Events recorded in the 5 minutes after the main sequence were important for engineering studies of strong earthquake ground motion, since their magnitudes ranged as high as 5.8, only 0.6 magnitude units smaller than the largest event in the main sequence. The rupture of the NW section of the fault may have taken place during an aftershock herein called the Brawley event, in agreement with an earlier suggestion by Richter (1958). The Tinemaha record of surface waves generated by the Brawley event, one hour and 17 minutes after the first event, illustrates the difference between surface waves from a simple event and those from the complicated main event.

(2) The seismic moment calculated for the main sequence of events, about 10^{26} dyne-cm, agrees well with the moment inferred from field observations of the fault offset.

(3) Two lines of evidence indicate that the seismic energy released in the first 15

seconds was generated by a series of events propagating SE from the vicinity of the initial epicenter along a section of the fault 25 km long:

(a) The Richter magnitude, M_L = 6.4, determined from stations NW of the epicenter was 0.7 magnitude units less than the surface wave magnitude, M_s = 7.1, determined from surface waves recorded SE and E of the epicenter. This suggests a focusing of energy toward the SE such as would be the expected for a rupture propagating in that direction.

(b) The distortion of the seismogram and moving window Fourier spectrum of surface waves at Tinemaha is consistent with a rupture propagating toward the SE.

(4) For the Imperial Valley earthquake, buildings with a relatively short fundamental period of oscillation (say, 1 sec and shorter) would respond as if the individual aftershock events were completely separate in time. Buildings with a relatively long fundamental period of oscillation (say 2 sec and longer) might vibrate with gradually increasing amplitude and thus the amount of damage could be closely related to the duration of the energy release in the whole sequence.

Acknowledgments

We wish to express our appreciation to Professors G. W. Housner, D. E. Hudson, and C. F. Richter for valuable discussion. They have also read the manuscript critically and offered many valuable suggestions. Mr. W. Cloud of USCGS kindly supplied us with a copy of the accelerogram record from El Centro strong motion station, of the Imperial Valley, California, 1940 earthquake. Professor C. Allen kindly provided the data for the measured field offset along the Imperial Valley fault given in Figure 9.

This study was supported by the National Science Foundation grant GP 1087 (Earthquake Mechanism) and National Science Foundation grant GK 1197X (Engineering Mechanics Program)

References

Aki, K. (1966). Generation and propagation of *G* waves from the Niigata earthquake of June 15, 1964, part 2. Estimation of the earthquake moment, release, energy, and stress-strain drop from the *G* wave spectrum. *Bull. Earthq. Res. Inst., Tokyo Univ.* **44**, 73–88.

Alford, J. L., G. W. Housner and R. R. Martel (1951). *Spectrum Analysis of Strong-Motion Earthquakes*, Earthq. Eng. Res. Lab., Calif. Inst. Tech.

Allen, C. R., A. Grantz, J. N. Brune, M. M. Clark, R. V. Sharp, T. G. Theodore, E. W. Wolfe and M. Wyss (1968). The Borrego Mountain, California, Earthquake of 9 April 1968: A preliminary report, *Bull. Seism. Soc. Am.* **58**, 1183–1185.

Ben-Menahem, A. and D. G. Harkrider (1964). Radiation patterns of seismic surface waves from buried dipolar point sources in a flat stratified Earth, *J. Geophys. Res.* **69**, 2605–2620.

Biehler, S. (1964). *Geophysical Study of the Salton Trough of Southern California*, Ph.D. Thesis, Calif. Inst. Tech.

Birch, F. (1961). The velocity of compressional waves in rocks to 10 kilobars, 2, *J. Geophys. Res.* **66**, 2199–2224.

Brune, J. N. (1968). Seismic moment, seismicity and rate of slip along major fault zones, *J. Geophys. Res.* **73**, 777–784.

Brune, J. N. and C. R. Allen (1967). A low-stress-drop, low magnitude earthquake with surface faulting: The Imperial, California, earthquake of March 4, 1966, *Bull. Seism. Soc. Am.* **57**, 501–514.

Brune, J. N. and G. R. Engen (1969). Excitation of mantle Love waves and definition of mantle wave magnitude, *Bull. Seism. Soc. Am.* **59**, 923–933.

Brune, J. N. and C. King (1967). Excitation of mantle Rayleigh waves of period 100 seconds as a function of magnitude, *Bull. Seism. Soc. Am.* **57**, 1355–1365.

Buwalda, J. P., Unpublished field notes (Prof. C. R. Allen).

Buwalda, J. P. and C. F. Richter (1941). Imperial Valley earthquake of May 18, 1940, *Bull. Geol. Soc. Am.* **52**, 1944 (Abstract).

Byerly, D. and J. M. De Noyer (1958). Energy in earthquakes as computed from geodetic observations [Chapter 2], Beinoff, V. H., and other eds., *Contributions in Geophysics: Internat. Ser. Mons. Earth Sci.* **1**, pp. 17–35.

Eaton, J. P. (1967). Instrumental seismic studies—the Parkfield-Cholame, California, earthquakes of June–August, 1966, *U. S. Geol. Survey Prof. Paper* **579**, pp. 57–65.

Florensov, N. A. and V. P. Solonenko (1963). *The Gobi-Altai Earthquake,* Isdatel'stvo Akademii Nauk SSR, Moscow, pp. 392.

Hamilton, R. M. and J. H. Healy (in press). Seismic activity associated with nuclear explosions.

Knopoff, L. (1958). Energy release in earthquakes, *Geophys. J.* **1**, 44–52.

Maruyama, T. (1963). On the force equivalent of dynamic elastic dislocations with reference to the earthquake mechanism, *Bull. Earthquake Res. Inst., Tokyo Univ.* **41**, 467–486.

Richter, C. F. (1958). *Elementary Seismology,* W. H. Freeman and Co., San Francisco.

Savage, J. C. (1965). The stopping phase on seismograms, *Bull. Seism. Soc. Am.* **55**, 47–58.

Ulrich, F. P. (1941). The Imperial Valley earthquakes of 1940. *Bull. Seism. Soc. Am.* **31**, pp. 13–31.

Wu, F. T. (1968). Parkfield earthquake of June 29, 1966; magnitude and source mechanism, *Bull. Seism. Soc. Am.* **58**, 689–709.

Wyss, M. and J. B. Brune (1967). The Alaska earthquake of 28 March 1964; A complex multiple structure, *Bull. Seism. Soc. Am.* **57**, 1017–1023.

Wyss, M. and J. N. Brune (1968). Seismic moment, stress and source dimensions for earthquakes in the California-Nevada region, *J. Geophys. Res.* **73**, 4681–4694.

Division of Engineering and Applied Science, and
Division of Geological Sciences
California Institute of Technology
Pasadena, California 91109
Contribution No. 1579

Manuscript received June 30, 1969.